C_1-Symmetric [Ir(C^N^1)(C^N^2)(O^O)]-*Tris*-Heteroleptic Iridium(III)-Complexes with the Preferentially Horizontal Orientation for High-Performance Near-Infrared (NIR) Organic Light-Emitting Diodes (OLEDs)

Wentao Li,[#] Baowen Wang,[#] Tiezheng Miao, Jiaxiang Liu, Xingqiang Lü,* Guorui Fu,* Linxi Shi, Zhongning Chen,* Pengcheng Qian,* and Wai-Yeung Wong*

Dr. Wentao Li, Baowen Wang, Tiezheng Miao, Jiaxiang Li, Guorui Fu, and Prof. Xingqiang Lü
School of Chemical Engineering, Northwest University, Xi'an 710069, Shaanxi, China
E-mail: lvxq@nwu.edu.cn
Dr. Linxi Shi and Prof. Zhongning Chen
State Key Laboratory of Structural Chemistry, Fujian Institute of Research on the Structure of Matter, Chinese Academy of Science, Fuzhou 350002, Fujian, China
F-mail: czn@fjirsm.ac.cn
Dr. Guorui Fu and Prof. Wai-Yeung Wong
Department of Applied Biology and Chemical Technology and Research Institute for Smart Energy, The Hong Kong Polytechnic University, Hung Hom, Hong Kong, China
E-mail: guorui.fu@polyu.edu.hk and wai-yeung.wong@polyu.edu.hk
Key Laboratory of Environment Functional Materials Technology and Applications of Wenzhou City, Institute of New Materials & Industry, College of Chemistry & Materials Engineering, Wenzhou University, Wenzhou 325035, Zhejiang, China
E-mail: qpc@wzu.edu.cn

Abstract

The development of high-efficiency NIR-emitting Ir(III)-complex-based phosphors for reliable NIR-OLEDs (near-infrared organic light-emitting diodes) is still a formidable challenge. Herein, a molecule-engineered approach is developed to afford three C_1-symmetric [Ir(C^N^1)(C^N^2)(O^O)]-*tris*-heteroleptic Ir(III)-complexes ([Ir(iqbt)(dFppy)(acac)] (**1**), [Ir(iqbt)(ppy)(acac)] (**2**) and [Ir(iqbt)(dpqx)(acac)] (**3**)), whose good NIR-luminescent efficiency (Φ_{PL} = 0.18 for **1** (λ_{em} = 703 nm), 0.26 for **2** (λ_{em} = 715 nm) or 0.28 for **3** (λ_{em} = 707 nm)) originates from the strengthened ^{3}MLCT contribution (MLCT = metal-to-ligand charge transfer). Moreover, the quantitative molecular orientation determination of their doped emitting layers (EMLs) reveals that the preferential horizontal orientation of the emitting dipoles is beneficial to their highly efficient NIR-OLEDs with light out-coupling. Especially for the **NIR-OLED-2** with λ_{em} = 715 nm, its high performance (η_{EQE}^{Max} = 5.30% and negligible (< 2%) efficiency-roll-off) among the reported solution-processed NIR-OLEDs based on Ir(III)-complexes at the similar color gamut is realized. This result shows that C_1-symmetric [Ir(C^N^1)(C^N^2)(O^O)]-*tris*-heteroleptic Ir(III)-complexes can provide a new platform to low-cost and large-area scalable NIR-OLEDs.

1. Introduction

Inspired by the emerging importance of near-infrared (NIR; λ_{em} > 700 nm) organic light-emitting diodes (OLEDs) in night-vision display,[1] information security,[2] optical telecommunication[3] and photodynamic therapy,[4] concrete efforts[5] have been devoted to the molecular design of NIR-emitters. In this regard, due to the concurrent harvesting of singlet and triplet excitons, NIR-emissive phosphors are more suitable candidates compared to fluorescent luminogens with an upper limit of the η_{IQE} (internal quantum efficiency) of 25%. Saliently for the octahedral Ir(III)-complexes with rather short triplet lifetimes, besides the high efficiency which is appreciably competitive to other triplet-based counterparts[5] (Pt(II)-complexes and TADF (thermal activated delayed fluorescence) molecules, etc.), the superiority of a significantly alleviated efficiency-roll-off renders them particular appealing[6] to the studies of NIR-OLEDs. Nonetheless, as constrained by the so-called "energy-gap law",[7] it remains a real challenge to develop new Ir(III)-complex dyes towards high-performance NIR-OLEDs.

To date, cyclometalated Ir(III)-complexes, possessing neutral ([Ir(C^N)$_3$]-homoleptic[8] or [Ir(C^N)$_2$(L^X)]-heteroleptic; L^X = O^O[9] or N^O[10]) and cationic ([Ir(C^N)$_2$(N^N)]$^+$)[11] forms and acting as both the chromophore and the charge-transport medium, were demonstrated for reliable NIR-OLEDs. Apparently, in order to narrow the HOMO-LUMO (HOMO = highest occupied molecular orbital; LUMO = lowest unoccupied molecular orbital) gap of a specific Ir(III)-complex towards the restrictive NIR emission, the use of π-conjugation expansion[8-11] of the C^N-cyclometalated main ligand, especially with electron-rich substituents, is generally preferred which can effectively destabilize the HOMO energy level. Considering the facile aggregation-caused quenching (ACQ)[12] effect arising from the large π-conjugation of the C^N-cyclometalated main ligand, modification of the HL^X ancillary ligand seems to be an accessible alternative way to stabilize the LUMO energy level of the [Ir(C^N)$_2$(L^X)]-heteroleptic[9-11] Ir(III)-complex. However, its exclusively reduced

HOMO-LUMO band-gap for NIR luminescence does not have an universal effect,[13] and even the undesirable hypsochromic shift[13] beyond the NIR regime results from the simultaneous stabilization of the HOMO energy level. Additionally, according to the "energy-gap law",[7] the inverse of k_{nr} (non-radiative rate constant) depends exponentially on the excited-state (^{1}T) energy, and k_r (radiative rate constant) has the cubic dependence. Therefore, high photo-luminescence efficiency necessary to increase k_r and/or to reduce k_{nr} is essential for obtaining the desired NIR emission. Convincingly, these two factors, which are key to reliable NIR-OLEDs, are highly associated with the specific excited state situations of the Ir(III)-complexes (such as energy-level and electron/charge transfer (CT) among the ^{3}MLCT/^{3}LC (LC = ligand-centered; MLCT = metal-to-ligand charge transfer) of the ^{1}T state, etc.).[14] In light of the transformation[15] of the ^{1}T nature in the C_1-symmetric *tris*-heteroleptic Ir(III)-complex composed of an Ir(III) ion and three different ligands, it is of notable interest on expanding that novel molecule-engineered strategy to Ir(III)-complex-based NIR-emitters, which should fill in the blank after previously reported NIR-emissive [Ir(C^N)$_3$]-[8] and [Ir(C^N)$_2$(L^X)]-heteroleptic[9-11] Ir(III)-complexes. Indeed, for C_1-symmetric *tris*-heteroleptic Ir(III)-complexes, their evident advantage lies in the potentially enriched inventory ([Ir(C^N^1)(C^N^2)(L^X)] (L^X = O^O or N^N),[15-16] [Ir(C^N^1)(C^N^2)(C^N^3)],[17] [Ir(C^N^1)(C^C^2)(C^N^3)],[18] [Ir(C^N^1)(N^N^1)(N^N^2)],[19] etc.) compared to conventional [Ir(C^N)$_3$]-[8] and [Ir(C^N)$_2$(L^X)]-counterparts.[9-11] Meanwhile, the breaking of the symmetry of molecular structures can help increasing the solubility of resultant Ir(III)-complexes. Moreover, arising from the C_1-symmetric *tris*-heteroleptic spatial configuration, the emitting dipole orientation (EDO) is rearranged. Especially through the specific multi-ligands' perturbation, the d-orbital participation in the ^{1}T state (^{3}MLCT contribution) can be redistributed. More importantly, for the emitting layers (EMLs) fabricated from C_1-symmetric *tris*-heteroleptic Ir(III)-complexes, the molecular orientation is further specified, offering a promise to boost the light-coupling efficiency.[20] Noticeably, although the effectiveness and

handiness of controlling the *fac*-[Ir(C^N)$_3$]-homoleptic[21] or [Ir(C^N)$_2$(L^X)]-heteroleptic[22] emitter's alignment parallel to the substrate, even without the need of micro-lens arrays, gratings or some other physical methods,[23] were demonstrated to significantly improve their visible-light out-coupling efficiency (η_{out}) by increasing the horizontal dipole ratio, this proof-of-concept approach has not been carried forward to Ir(III)-complex-based NIR-emitting systems.

Herein, encouraged by the smooth color-tuning[15-19] and good device performance[15] within the vivid visible (λ_{em} = 465-600 nm) range of C_1-symmetric *tris*-heteroleptic Ir(III)-complexes, it is anticipated that an attractive structural design strategy to our C_1-symmetric [Ir(C^N^1)(C^N^2)(O^O)]-*tris*-heteroleptic Ir(III)-complexes **1**-**3** (**Scheme 1**) could offer an opportunity to give NIR emission. Especially through the strengthened ^{3}MLCT effect from the C_1-symmetric spatial configuration, large k_r and/or reduced k_{nr} can be motivated toward the efficient NIR-phosphorescence. Accordingly, we also expect that the photo-physical and electrochemical properties of these NIR-emitting phosphors can be smoothly governed by varying the C^N^2 ligand. Moreover, owing to the lower symmetry of the molecular configuration of the Ir(III)-complexes **1**-**3** than typical C_3-symmetric-*fac*-[Ir(C^N)$_3$][21] and C_2-symmetric-[Ir(C^N)$_2$(L^X)][22] counterparts, it is believed that more preferential horizontal orientation of the C_1-symmetric [Ir(C^N^1)(C^N^2)(O^O)]-*tris*-heteroleptic Ir(III)-complexes should be beneficial for the NIR-light extraction[20] and challenging the low efficiency limited by the so-called "energy-gap law".[7] However, related study is not yet available for *tris*-heteroleptic Ir(III) complexes and was rarely reported for NIR systems. Thus, our present research renders the C_1-symmetric *tris*-heteroleptic Ir(III)-complexes a new platform to the realization of efficient NIR-OLEDs by utilizing their preferential horizontal orientation.

Scheme 1. Synthetic scheme of the C_1-symmetric [Ir(C^N^1)(C^N^2)(O^O)]-*tris*-heteroleptic Ir(III)-complexes **1**-**3** with different C^N^2-ligands.

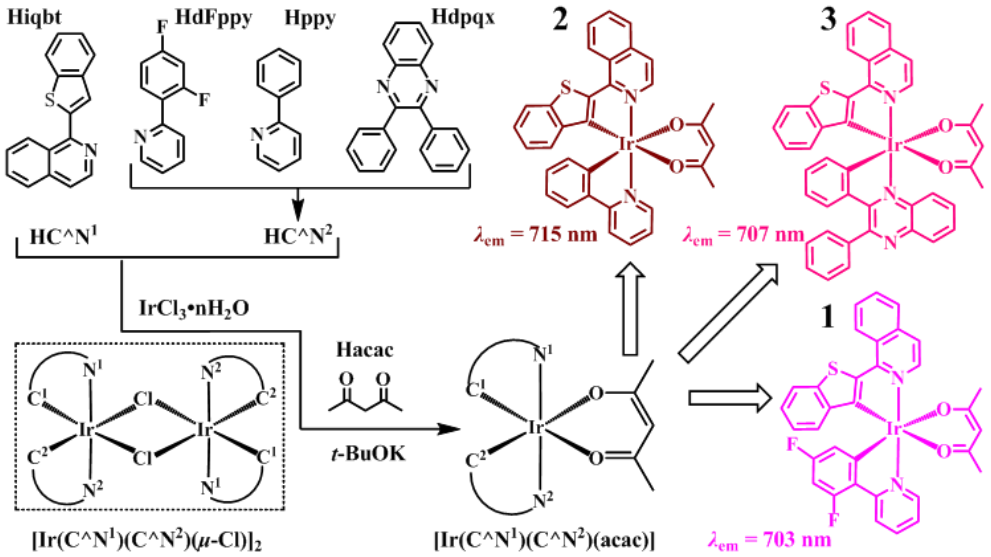

2. Results and Discussion

2.1. Synthesis and Characterization of C_1-Symmetric [Ir(C^N^1)(C^N^2)(O^O)]-*Tris*-Heteroleptic Ir(III)-Complexes 1-3

Suzuki coupling[10c] of cost-effective 2-Cl-isoquinoline (instead of 2-Br-isoquinoline[9e]) with benzo[*b*]thien-2-yl boronic acid gave the HC^N^1 main ligand **Hiqbt** in 73% yield. Also as shown in **Scheme 1**, straightforward metalation[15] in the 2-ethoxyethanol/H_2O (v/v = 3:1) mixed-solvent of the **Hiqbt** and one of the HC^N^2 ligands (**HdFppy**, **Hppy** and **Hdpqx**) in an equimolar ratio with $IrCl_3 \cdot 3H_2O$, gave rise to the corresponding *in situ* formed μ-chloro-bridged dimer intermediate [Ir(C^N^1)(C^N^2)(μ-Cl)]$_2$, which was not isolated from the inevitable interferents of [Ir(C^N^1)$_2$(μ-Cl)]$_2$ and [Ir(C^N^2)$_2$(μ-Cl)]$_2$. Further through the treatment of the μ-chloro-bridged dimer intermediates with **Hacac** in the presence of *t*-BuOK, the target C_1-symmetric [Ir(C^N^1)(C^N^2)(O^O)]-*tris*-heteroleptic Ir(III)-complex [Ir(iqbt)(dFppy)(acac)] (**1**), [Ir(iqbt)(ppy)(acac)] (**2**) or [Ir(iqbt)(dpqx)(acac)] (**3**) as the corresponding desirable product, was obtained upon the subsequent chromatography

separation, respectively. Undoubtedly, in synthesizing each of the corresponding C_1-symmetric [Ir(C^N^1)(C^N^2)(O^O)]-*tris*-heteroleptic Ir(III)-complexes **1**-**3**, two kinds of *bis*-heteroleptic Ir(III)-complexes [Ir(C^N^1)$_2$(O^O)] (the same [Ir(iqbt)$_2$(acac)]) and [Ir(C^N^2)$_2$(O^O)] ([Ir(dFppy)$_2$(acac)], [Ir(ppy)$_2$(acac)] or [Ir(dpqx)$_2$(acac)]) were also isolated as the by-products and structurally confirmed by spectroscopic characterization (shown in **ESI**), respectively. Worthy of note, probably contributing from the promoted solubility of the [Ir(C^N^1)(C^N^2)(O^O)]-*tris*-heteroleptic Ir(III)-complexes **1**-**3** with the C_1-symmetricity, their resultant yields (21-23%) after isolation are desirably acceptable.

The C_1-symmetric *tris*-heteroleptic Ir(III)-complexes, which are soluble in common organic polar or non-polar solvents, were well-characterized by elemental analysis, FT-IR, ^{1}H NMR and ESI-MS (see **ESI**). Especially in the ^{1}H NMR spectra (**Figure S1**) of the Ir(III)-complexes **1**-**3**, the proton resonances (δ = 5.71-9.02 ppm for **1**; 6.18-8.92 ppm for **2** and 6.27-9.10 ppm for **3**) of both the (**iqbt**)$^-$ and the corresponding (**dFppy**)$^-$/(**ppy**)$^-$/(**dpqx**)$^-$ ligands are presented. Moreover, different from the one set of proton signals (**Figure S2**) of the (**acac**)$^-$ in the C_2-symmetric [Ir(C^N^1)$_2$(O^O)]/[Ir(C^N^2)$_2$(O^O)], the H atoms on the two -CH_3 groups in every (**acac**)$^-$ ancillary ligand were split into two sets of singlet signals, peaking at 1.86 and 1.76 ppm for **1**, 1.74 and 1.68 ppm for **2** or 1.73 and 1.61 ppm for **3**, respectively, indicating the desirable destruction of structural symmetry.[15-19] The C_1-symmetric [Ir(C^N^1)(C^N^2)(O^O)]-*tris*-heteroleptic character of the representative Ir(III)-complex **2** was further confirmed by its X-ray crystallographic analysis (**Tables S1**-**2**). As depicted in **Figure 1**, one (**iqbt**)$^-$ ligand, one (**ppy**)$^-$ ligand with the similar C^N chelation (C11^N1 or C18^N2) mode and one (**acac**)$^-$ ancillary ligand with the O^O-chelate (O1^O2) mode coordinate to one Ir(III)-centre in a distorted octahedral geometry. Evidently, besides the O^O-chelation of the (**acac**)$^-$, the *cis*-C,C and *trans*-N,N dispositions of the two different C^N ligands ((**iqbt**)$^-$ and (**ppy**)$^-$) render the mononuclear Ir(III)-complex **2** comparable to the typical asymmetric [Ir(C^N^1)(C^N^2)(O^O)]-*tris*-heteroleptic Ir(III)-complexes.[15] TGA (thermogravimetric

analysis) result (**Figure S3**) of the Ir(III)-complexes **1-3** showed their good thermal stability with 5% weight-reduction temperature ($\Delta T_{5\%}$) over 300 °C, which is sufficient for the following solution-processed device fabrication.

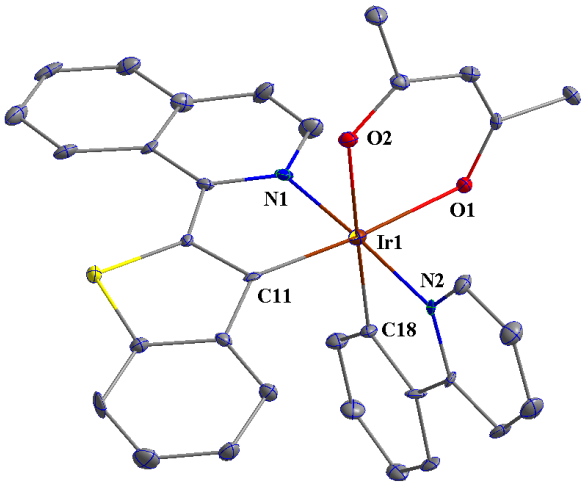

Figure 1. Perspective drawing of the C_1-symmetric [Ir(C^N^1)(C^N^2)(O^O)]-*tris*-heteroleptic framework in the Ir(III)-complex **2** using thermal ellipsoids at a 30% probability level. All the hydrogen atoms and most of the labels are omitted for clarity.

2.2. Photophysical Properties of the C_1-Symmetric Ir(III)-Complexes 1-3

The photophysical properties of the Ir(III)-complexes **1-3** measured in solution at room temperature were examined, and the results were summarized in **Table S3**. In contrast to the limited absorptions (λ_{ab} < 450 nm; **Figure S4**) of the C^N ligands and **Hacac**, the Ir(III)-complexes **1-3** exhibit the significantly broadened UV-visible-NIR absorption spectra (**Figure 2**), and besides the strong $^1\pi$-π^* absorption bands at the high-energy region (250-460 nm), the relatively weak absorptions in the lower-energy region (λ_{ab} > 470 nm) are tentatively assigned to the admixed ^{1,3}LC/^{1,3}MLCT (LC including LLCT (ligand-to-ligand charge transfer) and ILCT (intraligand charge transfer)) transitions. Nonetheless, the differential ^{1,3}LC/^{1,3}MLCT absorption behaviors (λ_{ab} = 508 nm for **1**, 525 nm for **2** or 603 nm for **3**) of the Ir(III)-

complexes **1-3**, as confirmed by their DFT (density functional theory) and time-dependent DFT (TD-DFT) calculations (*vide infra*), should result from the different electronic effects with specific $(C\hat{}N^2)^-$ ligands involved.

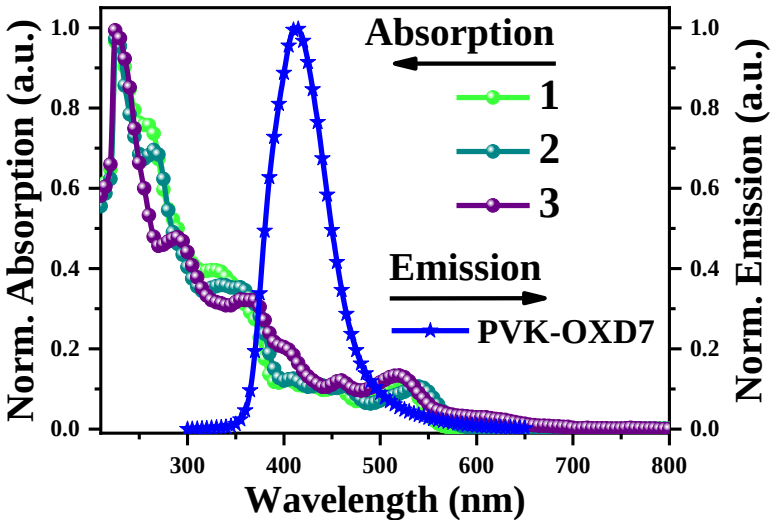

Figure 2. The normalized UV-visible-NIR absorption and emission spectra of the Ir(III)-complexes **1-3** in solution (λ_{ex} = 477 nm) and the PVK-OXD7 (65:30; weight ratio) in solid-state film (λ_{ex} = 273 nm) at room temperature, respectively.

Upon photo-excitation, in contrast to the rigidochromic fluorescence (**Figure S5**) of the ligands, all the three C_1-symmetric Ir(III)-complexes in CH_2Cl_2 solution emit the typical NIR emissions (**Figure 3**), peaking at 703 nm with a weaker shoulder at 779 nm for **1**, 715 nm and 768 nm (sh) for **2**, and 707 nm and 756 nm (sh) for **3**, respectively. The absence of the ligands' emissions should result from the efficient Dexter energy transfer[24] for the Ir(III)-complexes **1-3**. Meanwhile, their NIR-phosphorescent nature is further reflected from the corresponding T_1-decayed lifetime τ of 0.30 μs (**1**), 0.42 μs (**2**) or 0.45 μs (**3**). On one hand, the well-defined vibronic structure of their spectral profiles implies that the ^{3}LC-state should be substantially involved in the T_1 radiative decay for these NIR-emissive Ir(III)-complexes in addition to the ^{3}MLCT state. The almost no solvatochromic shift (**Figure S6**) of their NIR-

emissive bands in solvents of different polarities, together with the featureless FWHM (full width at half-maximum) up to *ca*. 70 nm, demonstrates their weak geometry distortion at the T_1 state. Moreover, in accordance with the calculated T_1 energy level order above, the NIR-emission maximum (λ_{em} = 715 nm) of the (**ppy**)$^-$-based Ir(III)-complex **2** exhibits a significant bathochromic shift compared with those (696-710 nm) of the previous C_2-symmetric [Ir(iqbt)$_2$(L^X)]-counterparts[9e,10c] or the other two C_1-symmetric Ir(III)-complexes **1** and **3** with the electron-withdrawing/enriching effects. As to the shortest lifetime unusually found for the (**dFppy**)$^-$-based Ir(III)-complex **1**, it may be due to the weaker vibrational nonradiative coupling effect with the relatively smaller Huang-Rhys factor (S_M)[25] of 0.29 than those (0.32-0.38) for the other Ir(III)-complexes **2**-**3**. Noticeably, contributing from the weak vibronic coupling (S_M = 0.29-0.38) between the T_1 and the S_0 states coupled with the distinctively shorter lifetimes (τ = 0.30-0.45 μs) of the C_1-symmetric [Ir(C^N^1)(C^N^2)(O^O)]-*tris*-heteroleptic Ir(III)-complexes **1**-**3** than those (τ ~ 1.0 μs) of conventionally C_2-symmetric [Ir(C^N)$_2$(L^X)]-counterparts,[9-11] their NIR-emissive efficiencies are significantly improved, exhibiting the Φ_{PL} = 0.18 for **1** (λ_{em} = 703 nm), 0.26 for **2** (λ_{em} = 715 nm) and 0.28 for **3** (λ_{em} = 707 nm), respectively. In good agreement with these results, their efficient NIR-phosphorescence is further confirmed from their six-fold increase in k_r values (6.00-6.22×10^5 s^{-1}). Excitingly, despite the fact that the situation is restricted to the so-called "energy gap law",[7] the augmented ^{3}MLCT-characters (21.17% (**2**); 20.76% (**3**)) of the Ir(III)-complexes **2**-**3** relative to that of 18.30% (**1**) are reflected, as also confirmed by their DFT/DT-DFT calculations (*vide infra*). Therefore, both the large k_r value and the relatively smaller k_{nr} (1.76×10^6 s^{-1}; also **Table S3**), engender the Ir(III)-complex **2** an attractive efficiency (Φ_{PL} = 0.26) even with the NIR-emission wavelength extending to 715 nm.

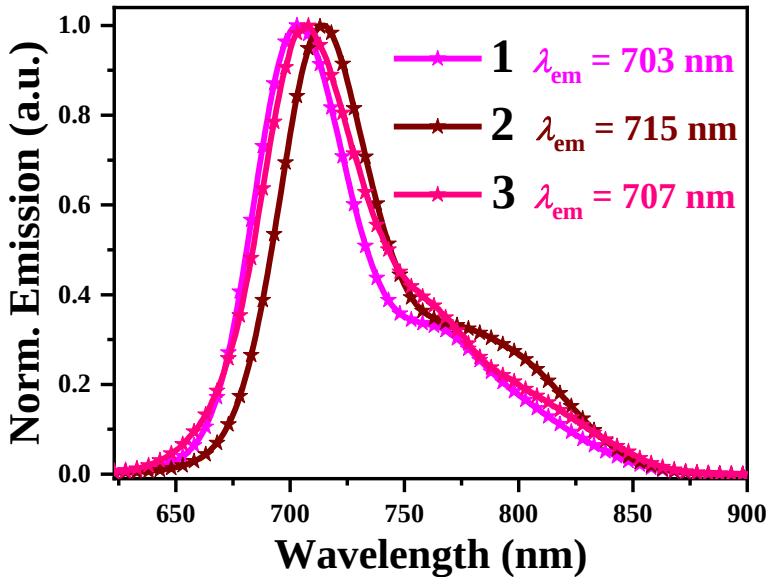

Figure 3. The normalized NIR emission spectra of the C_1-symmetric Ir(III)-complexes **1-3** in CH_2Cl_2 solution at room temperature.

2.3. Electronic Structure Calculations of the C_1-Symmetric Ir(III)-Complexes 1-3

To deeply understand the photophysical behaviors of the C_1-symmetric Ir(III)-complexes **1-3**, DFT/TD-DFT calculations based on their optimized S_0 and T_1 geometries were performed, respectively. According to the theoretical calculation results (**Tables S4-5** and **Figure 4**), the Ir(III)-complexes **1-2** have the similar distribution patterns to all the HOMOs and the LUMOs, where the most contribution (*ca*. 94%) from the C^N^2 ligand ((**dFppy**)$^-$ or (**ppy**)$^-$) to the LUMO+1 and the almost entire contribution (*ca*. 93%) from the C^N^1 ligand (**iqbt**)$^-$ to the LUMO, are observed, respectively. Moreover, besides the negligible (2.07% or 2.31%) contribution from the (**acac**)$^-$ ancillary ligand, the HOMO is mainly (63.88% or 56.42%) localized at the C^N^1 ligand (**iqbt**)$^-$ accompanied by some contributions from the Ir(III)-centre (25.06% or 28.31%) and the C^N^2 ligand (9.00% for (**dFppy**)$^-$ or 12.95% for (**ppy**)$^-$). Due to the electron-withdrawing effect, the (**dFppy**)$^-$-incorporation in the Ir(III)-complex **1** induces more contribution from the C^N^1 ligand (**iqbt**)$^-$ but with significantly reduced contribution

from the (**dFppy**)$^-$-C^N^2 ligand, the Ir(III)-centre and the (**acac**)$^-$ ancillary to the HOMO as compared with the (**ppy**)$^-$-based Ir(III)-complex **2**. However, the replacement of the C^N^2 ligand does not change the HOMO-1 pattern between the complexes **1**-**2**, revealing the domination (*ca*. 50%) from the (**acac**)$^-$ ancillary ligand, the substantial proportions from the Ir(III)-center (*ca*. 34%) and the C^N^1 ligand (**iqbt**)$^-$ (*ca*. 10%) and the minor fraction (*ca*. 4%) from the C^N^2 species. Therefore, considering the HOMO → LUMO transition (*ca*. 94%) featuring the S_1 state (also **Table S4**) of the Ir(III)-complexes **1**-**2**, although their low-energy UV-visible absorption is mainly caused by the ^{1}LC transition (^{1}ILCT (48.33%) and ^{1}LLCT (17.50%) for **1**; ^{1}ILCT (41.13%) and ^{1}LLCT (22.23%) for **2**) mixed with the ^{1}MLCT one (34.17% for **1**; 36.64% for **2**), the electron-withdrawing (**dFppy**)$^-$-incorporation stabilizes both the HOMO (-4.89 eV) and the LUMO (-1.89 eV) of its Ir(III)-complex **1** in comparison to those (-4.73 and -1.79 eV) of the Ir(III)-complex **2**, leading to the slightly broader HOMO-LUMO gap (E_g = 3.00 eV (**1**) versus 2.94 eV (**2**)), and thereby the blue-shifted (λ_{ab} = 508 nm (**1**) versus 525 nm (**2**)) low-energy absorption. Using the (**dpqx**)$^-$ with the larger π-conjugation as the C^N^2 ligand, its C_1-symmetric [Ir(C^N^1)(C^N^2)(O^O)]-*tris*-heteroleptic Ir(III)-complex **3** possesses a quite different HOMO/LUMO pattern from those of the Ir(III)-complexes **1**-**2**, in which besides the slightly increased contribution from the (**dpqx**)$^-$-C^N^2 ligand to the HOMO (14.12%) or the HOMO-1 (6.58%), the LUMO is almost entirely (94.58%) localized on the (**dpqx**)$^-$-C^N^2 ligand with the most contribution (93.47%) from the C^N^1 ligand (**iqbt**)$^-$ to the LUMO+1. Hence, for the Ir(III)-complex **3**, the low-energy UV-visible absorption showing the narrowest HOMO-LUMO gap (2.67 eV) with the distinctive bathochromic shift (λ_{ab} = 603 nm) is differentially originated from the ^{1}LLCT-dominated state ((C^N^2-ligand → C^N^1-ligand; 56.37%) among the ^{1}LLCT/^{1}MLCT/^{1}ILCT-admixture. Interestingly, despite the large contribution (*ca*. 89%) from the HOMO → LUMO transition to the corresponding T_1 state (1.775 eV (698 nm) of **1**; 1.748 eV (709 nm) of **2**) for the Ir(III)-complexes **1**-**2** while the HOMO → LUMO+1 transition to that (1.754 eV (707 nm)) of the Ir(III)-complex **3**, their

$S_0 \rightarrow T_1$ absorption transitions (also **Table S5**) are consistent and reasonably assigned to the admixed ^{3}LC/^{3}MLCT-transitions with the ^{3}ILCT-domination.

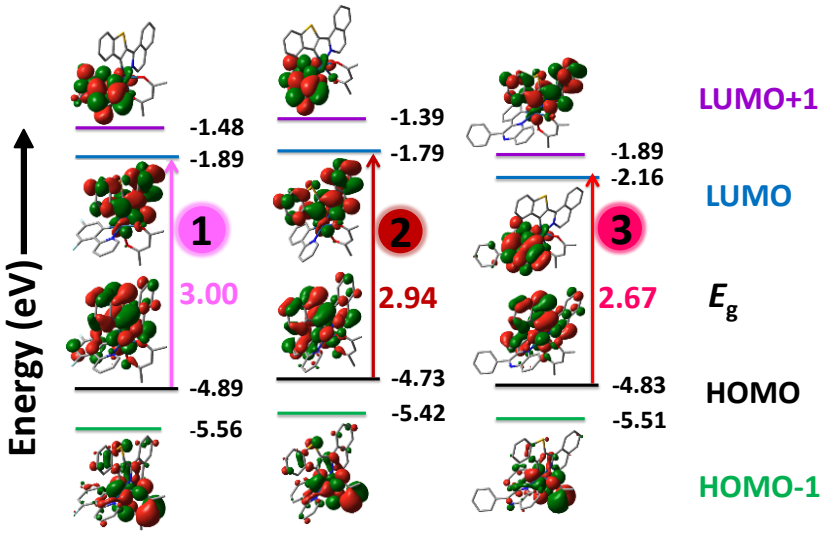

Figure 4. The HOMO and LUMO patterns for the C_1-symmetric Ir(III)-complexes **1-3** based on their corresponding optimized S_0 geometries.

NTO (natural transition orbital) calculations of the three C_1-symmetric Ir(III)-complexes **1-3** on optimized T_1 geometries were carried out to further elucidate their NIR-emissive behaviors. The NTO analysis (**Table S6** and **Figure 5**) shows that both the hole (*ca*. 84%) and the particle (*ca*. 92%) orbitals are dominated by the C^N^1 (**iqbt**)$^-$ ligand for each of the C_1-symmetric Ir(III)-complexes **1-3**, and the introduction of the (**ppy**)$^-$-C^N^2 ligand gives the significantly increased percentage on the d_π orbital of the Ir(III) centre for the Ir(III)-complex **2**. Nevertheless, based on the entire (100%) hole → particle transition, the ^{3}ILCT-dominated (78.10% for **1**; 73.82% for **2**; 72.79% for **3**; also **Table S5**) and the less prevalent ^{3}MLCT (18.30% for **1**; 21.17% for **2**; 20.76% for **3**) transition should be responsible for their well-structured NIR-emissive phosphorescence.

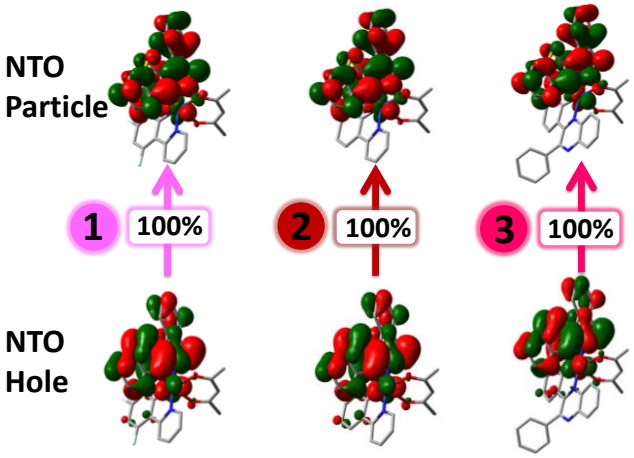

Figure 5. The NTO (natural transition orbital) hole and particle patterns for the C_1-symmetric Ir(III)-complexes **1**-**3** based on their optimized T_1 geometries.

Further considering the transition dipole effect from the attractive C_1-symmetry of the Ir(III)-complexes **1**-**3**, both the $\vec{\mu}$-S_0 *and* $\vec{\mu}$-T_1 dipole moments of the C_1-symmetric Ir(III)-complexes **1**-**3** and the C_3-symmetric *fac*-[Ir(iqbt)$_3$][26] or the C_2-symmetric [Ir(iqbt)$_2$(dpm)][9e] with the record-high η_{EQE}^{Max} = 3.07% (λ_{em} = 714 nm) were explored for comparison upon the DFT calculations from their corresponding optimized T_1 and S_0 states, respectively. As summarized in **Table S7** and **Figures 6** and **S7**, significantly different from the directions of the $\vec{\mu}$-S_0 *and* $\vec{\mu}$-T_1 dipole moment vectors located at the C_2-axis of the C_2-symmetric [Ir(iqbt)$_2$(dpm)][9e], the angle (θ; 32.44° (**1**), 34.83° (**2**) or 114.83° (**3**) between the two vectors is found for each of the C_1-symmetric Ir(III)-complexes **1**-**3** and larger than that (23.17°) of the C_3-symmetric *fac*-[Ir(iqbt)$_3$][26]. Accordingly, their transition dipole moment (TDM, $\Delta\vec{\mu}$ (T_1-S_0); 2.20 D (**1**), 2.36 D (**2**) and 3.60 D (**3**)) values are larger than that (2.01 D) of the C_3-symmetric-*fac*-[Ir(iqbt)$_3$][26] and 4-5 times larger than that (0.56 D) of the C_2-symmetric-[Ir(iqbt)$_2$(dpm)][9e]. However, despite the transition dipole orientation available for the Ir(III)-complexes **1**-**3** with the C_1-symmetry, the hypothesis of their anisotropically oriented EMLs needs to be further verified (*vide infra*).

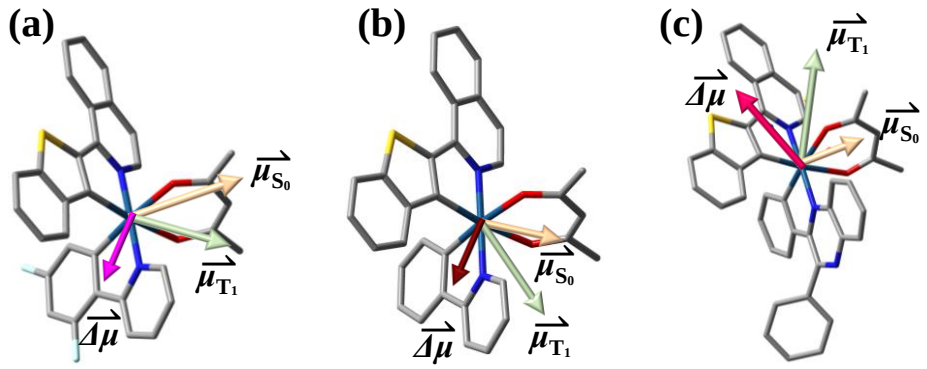

Figure 6 Chemical structure and TDMs (transition dipole moments) of the C_1-symmetric Ir(III)-complexes **1**-**3** by DFT calculations.

2.4. Electrochemical Properties of the C_1-Symmetric Ir(III)-Complexes 1-3 with Different C^N^2-Ligands

Based on the electrochemical behaviours (**Figure 7**), all the C_1-symmetric [Ir(C^N^1)(C^N^2)(O^O)]-*tris*-heteroleptic Ir(III)-complexes **1**-**3** exhibit a reversible oxidation wave at 0.48 eV (**1**), 0.37 eV (**2**) or 0.46 eV (**3**), respectively. The redox process (HOMO level stabilization; also shown in **Table S4** and **Figure 4**) can be mainly attributed to the oxidation of the benzothiophene unit of the C^N^1 ligand (**Hiqbt**) besides the Ir(III) centre involved. Clearly, in comparison to the Ir(III)-complex **2** or **3**, the stronger anodic shift (0.48 eV) in oxidation of the Ir(III)-complex **1** should result from the electron-withdrawing effect of two F atoms on the dFppy ligand. Meanwhile, owing to the (**ppy**)$^-$-C^N^2-induced stronger ^{3}MLCT effect, the higher electron density to the Ir(III) centre of the Ir(III)-complex **2** should be the reason to its lower oxidation potential (0.37 eV) than those (0.46-0.48 eV) of the Ir(III)-complexes **1** and **3**. Accordingly, both the HOMO (-4.77 eV) and LUMO (-2.63 eV) of the Ir(III)-complex **2** are destabilized in comparison with those (-4.88 and -2.65 eV for **1**; -4.86 and -2.98 eV for **3**) of the other two Ir(III)-complexes, through which a much narrower

experimental HOMO-LUMO band-gap (1.88 eV) of the Ir(III)-complex **3** well verifies its red-shifted low-energy absorption.

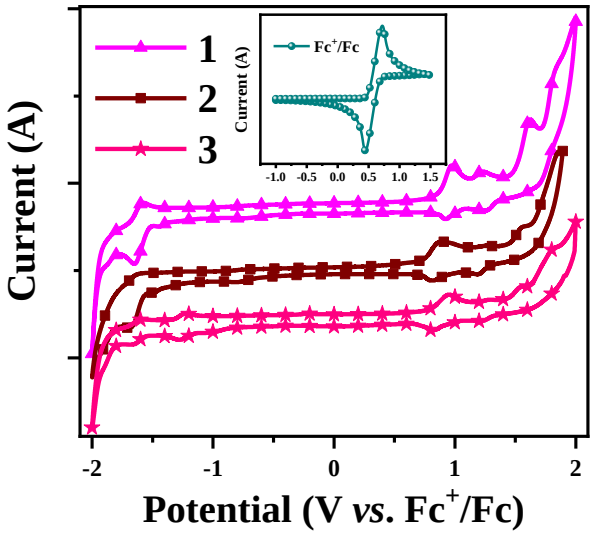

Figure 7. The cyclic voltammogram (CV) results of the Ir(III)-complexes **1-3** recorded versus Fc^+/Fc in solution at room temperature under a N_2 atmosphere (scan rate = 100 mV/s).

2.5. Device Performance of NIR-OLEDs Using the *C*$_1$-Symmetric Ir(III)-Complexes 1-3 with Different C^N^2-Ligands as the Dopants

Since the practical LUMO (-2.98 to -2.63 eV) and HOMO (-4.88 to -4.77 eV) energy levels of the C_1-symmetric [Ir(C^N^1)(C^N^2)(O^O)]-*tris*-heteroleptic Ir(III)-complexes **1-3** as the dopants fit perfectly within those (-3.00 to -2.00 eV of LUMO and -6.30 to -5.50 eV of HOMO) of the PVK-OXD7 (PVK = poly(*N*-vinylcarbazole); OXD7 = 1,3-bis(5-(4-*tert*-butyl-phenyl)-1,3,4-oxadiazol-2-yl)benzene), the PVK-OXD7 with good carrier transport should be the suitable *co*-host for their solution-processed NIR-OLEDs. Moreover, considering the significant spectral overlap (also **Figure 2**) between the blue-light (λ_{em} = 414 nm) emission of the *co*-host and the LLCT/MLCT absorption of the dopants, effective Förster energy transfer[27] should be motivated from the PVK-OXD7 to the Ir(III)-complex species upon the electrical excitation. Through the solution-processed procedure with the same configuration

depicted in **Figure 8(a)**, a series of NIR-OLEDs using the Ir(III)-complexes **1**-**3** as the dopants at a 5 wt% doping level in PVK-OXD7 (65:30, wt%) were fabricated. PEDOT:PSS (poly(ethylenedioxythiophene):poly(styrenesulfonate)) acted as the hole-injecting material.

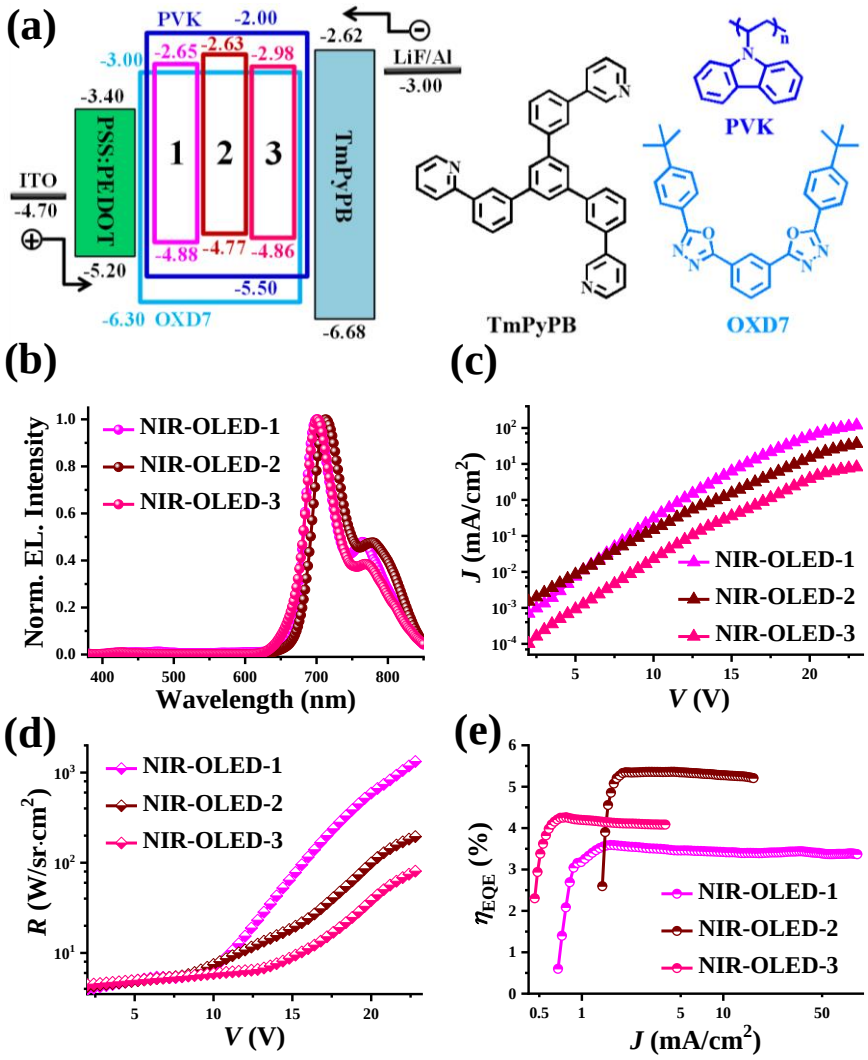

Figure 8. a) Device structures and energy level diagrams; b) normalized electroluminescent spectra; c) *J*-*V* (current density versus voltage); d) *R*-*V* (radiance versus voltage) and e) η_{EQE}-*J* (external quantum efficiency versus current density) curves based on NIR-OLEDs from the C_1-symmetric Ir(III)-complexes **1**-**3**.

In order to verify the effective charge transport of the *co*-host PVK-OXD7, hole-only and electron-only devices were fabricated with the configurations of ITO/MoO_3 (3 nm)/ PEDOT:PSS (40 nm)/PVK-OXD7 (65:30; weight ratio) (50 nm)/MoO_3 (3 nm)/Al (100 nm) and ITO/LiF (3 nm)/OXD7 (50 nm)/LiF (3 nm)/Al (100 nm), respectively. Meanwhile, based on the *J*–*V* curves (**Figure S8**) of the hole-only and electron-only devices, the hole/electron mobility was checked using the space-charge-limited current (SCLC) method. Accordingly, the hole mobility of PVK-OXD-7 was calculated to be *ca*. 1.62×10^{-6} cm^2 V^{-1} s^{-1}, which is slightly larger than the electron mobility (2.11×10^{-7} cm^2 V^{-1} s^{-1}) of OXD-7. Clearly, towards a desirable charge transport balance, an extra layer of TmPyPB (1,3,5-tri[(3-pyridyl)-phen-3-yl]benzene) serving as the interface-modified function[28] of both electron-transporting and hole-blocking, is necessary to ensure the good electroluminescent performance of the resultant NIR-OLEDs.

As shown in **Table S8** and **Figure 8(b)**, all the devices, upon illumination, exhibit the NIR electroluminescent spectra that well resembled the corresponding T_1-based photoluminescence profiles (also **Figure 3**) of the Ir(III)-complexes **1**-**3**, indicating that the Dexter energy transfer with their corresponding T_1 state should be the major process[24] despite the fact that the *co*-host to guest Förster energy transfer[27] occurred. Moreover, under a proper forward bias, the respective electroluminescent spectra are independent of the applied voltages. By further checking the *J*-*V*, *R*-*V* and η_{EQE}-*J* curves shown in **Figures 8(c-e)** for the **NIR-OLED-1/2/3**, in contrast to the monotonous increase of the *J* or *R* with increasing the applied bias voltage, the η_{EQE} in each case increases instantly and then decreases steadily throughout the whole illumination. For the **NIR-OLED-1** (λ_{em} = 703 nm), after application of 6.5 V of the V_{on} (the voltage of R = 5 W/sr·cm^2), it displays an η_{EQE}^{Max} of 3.59% with the R = 16 W/sr·cm^2 at the J = 1.18 mA/cm^2. As to the other NIR-OLEDs based on the Ir(III)-complexes **2** (λ_{em} = 715 nm) and **3** (λ_{em} = 705 nm), despite the distinctively lower R^{Max} (201

W/sr·cm^2 for the **NIR-OLED-2** upon V_{on} = 7.2 V and 84 W/sr·cm^2 upon V_{on} = 8.1 V for the **NIR-OLED-3**) than that (R^{Max} = 1400 W/sr·cm^2) of the **NIR-OLED-1**, the η_{EQE}^{Max} values of 5.30% for the **NIR-OLED-2** and 4.24% for the **NIR-OLED-3** are significantly larger than that (3.59%) of the **NIR-OLED-1,** mirroring their trend in the photo-excited Φ_{PL} (0.18 (**1**), 0.26 (**2**) and 0.28 (**3**)). The slightly higher V_{on} of 8.1 V for the **NIR-OLED-3** than those (6.5-7.2 V) of the other **NIR-OLEDs-1-2**, should be caused by the larger LUMO energy barrier (0.36 eV) between the emitter **3** and TmPyPB. Nonetheless, profiting from the short T_1-decayed lifetimes (τ = 0.30-0.45 μs), there is an almost negligible efficiency-roll-off (< 2%) for each of the three NIR-OLEDs.

Considering the record-high η_{EQE}^{Max} = 3.07% (λ_{em} = 714 nm) for the C_2-symmetric [Ir(iqbt)$_2$(dpm)][9e] doping in the PVK-OXD7 while the cathode Ba (7 nm)/Al (100 nm) was used, it is of particular interest on its scientific comparison with the C_1-symmetric [Ir(C^N^1)(C^N^2)(O^O)]-*tris*-heteroleptic Ir(III)-complexes **1-3**. Through the same device structure as the **NIR-OLED-1/2/3**, the [Ir(iqbt)$_2$(dpm)]-doped reference device was fabricated, and its electroluminescent behaviour (also **Table S8**) was shown in **Figure S9**. Despite the replacement of TmPyPB (45 nm)/LiF (1 nm)/Al (100 nm), the [Ir(iqbt)$_2$(dpm)]-doped reference device gave the almost identical η_{EQE}^{Max} = 3.46% (λ_{em} = 711 nm) to that[9e] with the cathode Ba (7 nm)/Al (100 nm). However, their inferior electroluminescent performance (η_{EQE}^{Max} = 3.07-3.46% and ~10% efficiency-roll-off) relative to those (η_{EQE}^{Max} = 3.59-5.30% and negligible (< 2%) efficiency-roll-off) of the **NIR-OLED-1/2/3** fabricated from the C_1-symmetric [Ir(C^N^1)(C^N^2)(O^O)]-*tris*-heteroleptic Ir(III)-complexes **1-3** is evident.

2.6. Effect of the Preferential Horizontal Orientation on the Enhanced Out-Coupling Efficiency of the NIR-OLEDs-1-3

Intriguingly, as compared with those solution-processed devices from the typical C_3-symmetric-*fac*-[Ir(C^N)$_3$][8] and C_2-symmetric [Ir(C^N)$_2$(L^X)]-counterparts,[9-11] the significantly improved electroluminescent performance of the **NIR-OLEDs-1-3** fabricated from the C_1-symmetric [Ir(C^N^1)(C^N^2)(O^O)]-*tris*-heteroleptic Ir(III)-complexes **1-3** are highlighted. According to the theoretical equation 1,

$$\eta_{EQE} = \eta_{eh} \times \eta_{PL} \times \eta_{exciton} \times \eta_{out} \quad (1)$$

η_{eh} is the recombination efficiency of injected holes and electrons, η_{PL} is the radiative emitter's quantum yield, $\eta_{exciton}$ is the radiative exciton ratio and η_{out} is the light out-coupling efficiency, the high efficiency (η_{EQE}^{Max} = 3.59% of the **NIR-OLED-1**; 5.30% of the **NIR-OLED-2**; 4.24% of the **NIR-OLED-3)** of our cases should inherently benefit from their inherent high quantum yield (Φ_{PL} = 0.18 for **1** (λ_{em} = 703 nm); 0.26 for **2** (λ_{em} = 715 nm); 0.28 for **3** (λ_{em} = 707 nm)) associated with the weak vibrational nonradiative coupling effect.[25] Meanwhile, relying on the suitable TmPyPB-interfaced[28] HOMO/LUMO-level alignment (also **Figure 8(b)**) towards the enhanced carrier injection/transport, more ^{1}T-excitons' confinement and recombination should be in a subordinate position. Especially contributing to the TmPyPB-induced negligible electron injection/transport barrier for the **NIR-OLED-2**, the desirable carrier balance might take into effect to give a better performance than that of the **NIR-OLED-3**. More importantly, even assuming the η_{eh} of 100% and the $\eta_{exciton}$ of 100%,[29] the calculated η_{out} of 20.0% for the **NIR-OLED-1**, 20.4% for the **NIR-OLED-2** or 15.1% for the **NIR-OLED-3** means that molecular orientation of the C_1-symmetric [Ir(C^N^1)(C^N^2)(O^O)]-*tris*-heteroleptic Ir(III)-complexes **1-3** in the EMLs should be beneficial for the NIR-light extraction.[20-22]

To further confirm this hypothesis, the quantitative orientation distribution of the EMLs doped with the C_1-symmetric Ir(III)-complexes **1-3** was experimentally determined by variable-angle spectroscopic ellipsometry (VASE) method.[30] Based on the following equations of the horizontal dipole ratio $h/(h + v)$ and the order parameter S relative to the

TDMs' anisotropy, respectively,

$$\frac{h}{h+v} = \frac{2(1-S)}{3} \qquad (2)$$

$$S = \frac{3(\cos^2\theta)-1}{2} = \frac{k_e^{max} - k_o^{max}}{k_e^{max} + 2k_o^{max}} \qquad (3)$$

where S (defined by the θ angle between the the transition dipole moment vector and the direction vertical to the substrate, or the ordinary and extraordinary coefficients k_o and k_e) of 0, -0.5 or 1 represents the isotropic, completely horizontal or vertical alignment to the substrate, respectively. As shown in **Figure 9**, both the ordinary refractive index (n_o) and the extraordinary refractive index (n_e) of the EMLs-**1**-**3** are highly sensitive to the wavelength of light, while their large values even at the corresponding emissive wavelength (1.637 and 1.661 at 703 nm (EML-**1**); 1.644 and 1.634 at 715 nm (EML-**2**); 1.683 and 1.648 at 707 nm (EML-**3**)) indicate that each of the EMLs-**1**-**3** should be horizontally orientated.[31] Moreover, their θ angles are up to 56.21-62.54°. Accordingly, their S (-0.036 of the EML-**1**; -0.073 of the EML-**2** or -0.181 of the EML-**3**) and the corresponding $h/(h + v)$ (exceeding 69%; 69.0%, 71.5% or 78.7%) results are summarized in **Table S9**, where the preferential orientation parallel to the substrate[20-22,30] for all the EMLs-**1**-**3** contributes to the high efficiency of their **NIR-OLEDs-1-3**. Worthy of note, the **NIR-OLED-2**, probably with the best overall optoelectronic properties, represents the most efficient one (η_{EQE}^{Max} = 5.30%; λ_{em} = 715 nm) among other solution-processed NIR-OLEDs[9a,9c-9(f),9(i),10-11] based on Ir(III)-complexes (**Table S10** and **Figure 10**). Besides the superiorities on cost-effectiveness and large-area, its satisfactory performance (high-efficiency and low efficiency-roll-off; λ_{em} = 715 nm), to the best of our knowledge, can even compete with those from vacuum-deposited NIR-OLEDs[8,9(b),9(g)-9(h)] based on Ir(III)-complexes.

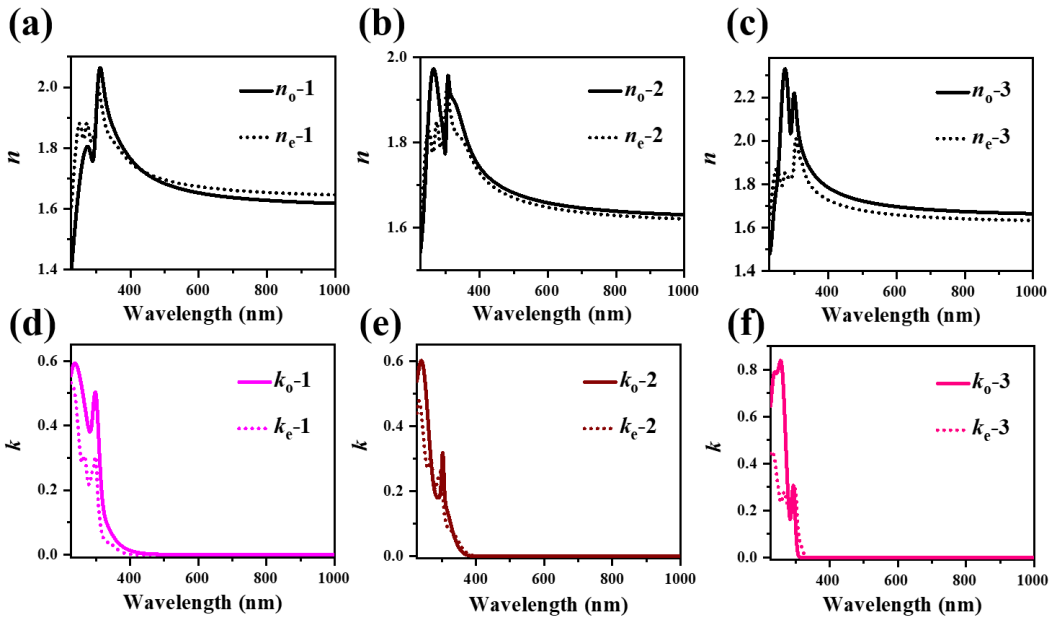

Figure 9. Wavelength-relative refractive indices (*n*; a-c) and coefficients (*k*; d-f) in ordinary (n_o/k_o) and extraordinary modes (n_e/k_e) of the EMLs doped with the corresponding C_1-symmetric Ir(III)-complexes **1**-**3**.

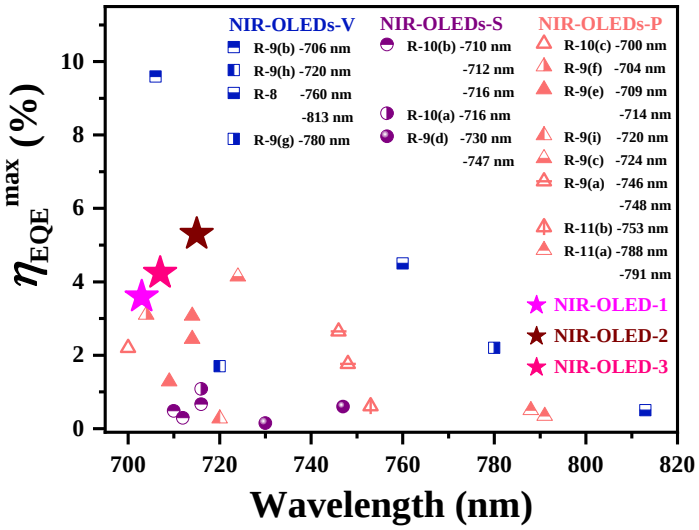

Figure 10. The λ_{EL}-relative η_{EQE} comparison between the **NIR-OLEDs-1/2/3** in this work with previously reported Ir(III)-complex-based vacuum-deposited NIR-OLEDs (NIR-OLEDs-V) and solution-processed small-molecule-hosted NIR-OLEDs (NIR-OLEDs-S) or polymer-hosted NIR-OLEDs (NIR-OLEDs-P).

3. Conclusions

In conclusion, through the C_1-symmetric [Ir(C^N^1)(C^N^2)(O^O)]-*tris*-heteroleptic molecular design strategy, the Ir(III)-complexes **1-3** showing the ^{3}LC/^{3}MLCT-admixed NIR-phosphorescence have been successfully obtained. The electronic effects endowed by different (C^N^2)-ligands can govern the color-tuning within the NIR (λ_{em} = 703-715 nm) region to some extent. Moreover, as a result of their doped polymer films with the preferential horizontal orientation for reliable solution-processed NIR-OLEDs, the attractive device performance especially with the η_{EQE}^{Max} (λ_{em} = 715 nm) up to 5.30% is the best among solution-processed NIR-OLEDs and even comparable to those of vacuum-deposited NIR-OLEDs fabricated from Ir(III)-complexes with the similar NIR-emissive gamut. This result offers Ir(III)-complex featuring a C_1-symmetric [Ir(C^N^1)(C^N^2)(O^O)]-*tris*-heteroleptic structure a new platform to efficient NIR-OLEDs.

Supporting Information

Electronic Supporting Information including experimental details, synthesis and characterization, and supplemental Tables and Figures is available from the Wiley Online Library or from the author.

Acknowledgements

X. Lü thanks the National Natural Science Foundation (21373160 and 21173165) and the State Key Laboratory of Structure Chemistry (20190026) in China. Z. Chen thanks the National Natural Science Foundation (21801242 and 21701171) in China. W.-Y. Wong thanks the Hong Kong Research Grants Council (PolyU153058/19P), Guangdong-Hong Kong-Macao Joint Laboratory of Optoelectronic and Magnetic Functional Materials (2019B121205002), the Hong Kong Polytechnic University (1-ZE1C and YW4T), Research

Institute for Smart Energy (RISE) and the Endowed Professorship in Energy from Ms. Clarea Au (847S). Dr. P. Qian thanks the Foundation of Wenzhou Science & Technology Bureau (W20170003) and the National Natural Science Foundation of China (21828102).

Conflict of Interest

The authors declare no conflict of interest.

[#]These authors contributed equally and should be considered *co*-first authors.

Keywords

Cyclometalated Ir(III)-complex, *tris*-heteroleptic configuration, transition dipole moment; near-infrared phosphorescence, solution-processed organic light-emitting diode

References

[1] L. T. Dou, Y. S. Liu, Z. R. Hong, G. Li, Y. Yang, *Chem. Rev.* **2015**, *115*, 12633-12665.

[2] A. Rogalski, K. Chrzanowski, *Opto-Electron. Rev.* **2002**, *10*, 111-136.

[3] (a) J. Clark, G. Lanzani, *Nat. Photon.* **2010**, *4*, 438-446; (b) J.-C. G. Bünzli, S. V. Eliseeva, *J. Rare Earths* **2010**, *28*, 824-842.

[4] (a) F. Ding, Y. Fan, Y. Sun, F. Zhang, *Adv. Healthcare Mater.* **2019**, *8*, 1900260; (b) S. V. Eliseeva, J.-C. G. Bünzli, *Chem. Soc. Rev.* **2010**, *39*, 189-227.

[5] (a) A. Zampetti, A. Minotto, F. Cacialli, *Adv. Funct. Mater.* **2019**, *29*, 1807623; (b) L. D. Wang, Z. F. Zhao, C. Wei, Z. W. Liu, Z. Q. Bian, C. H. Huang, *Adv. Opt. Mater.* **2019**, *7*, 1801256; (c) J. H. Kim, J. H. Yun, J. Y. Lee, *Adv. Opt. Mater.* **2018**, *6*, 1800255; (d) C.-L. Ho, H. Li, W.-Y. Wong, *J. Organomet. Chem.* **2014**, *751*, 261-285; (g) H. F. Xiang, J. H. Cheng, X. F. Ma, X. G. Zhou, J. J. Chruma, *Chem. Soc. Rev.* **2013**, *42*, 6128-6185.

[6] (a) M. Ibahim-Ouali, F. Dumur, *Molecules* **2019**, *24*, 1412; (b) Y. M. Zhang, Y. F. Wang, J. Song, J. L. Qu, B. H. Li, W. G. Zhu, W.-Y. Wong, *Adv. Opt. Mater.* **2018**, *6*, 1800466.

[7] J. V. Caspar, T. J. Meyer, *J. Phy. Chem.* **1983**, *87*, 952-957.

[8] J. Xue, L. J. Xin, J. Y. Hou, L. Duan, R. J. Wang, Y. Wei, J. Qiao, *Chem. Mater.* **2017**, *29*, 4775-4782.

[9] (a) D. H. Liu, C. F. You, M. K. Li, S. Wang, K. Zhang, B. Zhang, J. T. Yu, Y. Liu, S. J. Su, W. G. Zhu, *J. Organomet. Chem.* **2021**, *931*, 121615; (b) Z. Chen, H. Y. Zhang, D. W. Wen, W. H. Wu, Q. G. Zeng, S. M. Chen, W.-Y. Wong, *Chem. Sci.* **2020**, *11*, 2342-2349; (c) C. F. You, D. H. Liu, F. Y. Meng, Y. F. Wang, J. T. Yu, S. Wang, S. J. Su, W. G. Zhu, *J. Mater. Chem. C* **2019**, *7*, 10961-10971; (d) H. U. Kim, S. Sohn, W. Choi, M. Kim, S. U. Ryu, T. Park, S. Jung, K. S. Bejoymohandas, *J. Mater. Chem. C* **2018**, *6*, 10640-10658; (e) S. Kesarkar, W. Mróz, M. Penconi, M. Pasini, S. Destri, M. Cazzaniga, D. Ceresoli, P. R. Mussini, C. Baldoli, U. Giovanella, A. Bossi, *Angew. Chem. Int. Ed.* **2016**, *55*, 2714-2718; (f) X. S. Cao, J. S. Miao, M. R. Zhu, C. Zhong, C. L. Yang, H. B. Wu, J. G. Qin, Y. Cao, *Chem. Mater.* **2015**, *27*, 96-104; (g) R. Tao, J. Qiao, G. L. Zhang, L. Duan, C. Chen, L. D. Wang, Y. Qiu, *J. Mater. Chem. C* **2013**, *1*, 6446-6454; (h) J. Qiao, L. Duan, L. T. Tang, L. He, L. D. Wang, Y. Qiu, *J. Mater. Chem.* **2009**, *19*, 6573-6580; (i) E. L. Williams, J. Li, G. E. Jabbour, *Appl. Phys. Lett.* **2006**, *89*, 083506.

[10] (a) H. U. Kim, H. J. Jang, W. Choi, S. Park, T. Park, J. Y. Lee, K. S. Bejoymohandas, *J. Mater. Chem. C* **2020**, *8*, 4789-4800; (b) J. T. Yu, C. Xu, F. Y. Meng, H. Tan, M. Q. Liu, W. G. Zhu, *Dyes Pigm.* **2019**, *166*, 307-313; (c) G. R. Fu, H. Zheng, Y. N. He, W. T. Li, X. Q. Lü, H. S. He, *J. Mater. Chem. C* **2018**, *6*, 10589-10596.

[11] (a) L. J. Xin, J. Xue, G. T. Lei, J. Qiao, *RSC Adv.* **2015**, *5*, 42354-42361; (b) R. Tao, J. Qiao, G. L. Zhang, L. Duan, L. D. Wang, Y. Qiu, *J. Phys. Chem. C* **2012**, *116*, 11658-11664.

[12] A. F. Henwood, E. Zysman-Colman, *Chem. Commun.* **2017**, *53*, 807-826.

[13] G. N. Li, Y. Zhou, Y. D. Yang, J. Liang, F. Cui, T. Zheng, H. Xie, Z. G. Niu, *J. Fluoresc.* **2014**, *24*, 1545-1552.

[14] T. Y. Li, J. Wu, Z. G. Wu, Y. X. Zheng, J. L. Zuo, Y. Pan, *Coord. Chem. Rev.* **2018**, *374*, 55-92.

[15] (a) Y. H. Sun, X. L. Yang, B. O. Liu, J. S. Dang, Y. Li, G. J. Zhou, Z. X. Wu, W.-Y. Wong, *J. Mater. Chem. C* **2019**, *7*, 8836-8846; (b) X. L. Yang, Z. Feng, J. S. Dang, Y. H. Sun, G. J. Zhou, W.-Y. Wong, *Mater. Chem. Front.* **2019**, *3*, 376-384;(c) Y. H. Sun, X. L. Yang, Z. Feng, B. O. Liu, D. K. Zhong, J. J. Zhang, G. J. Zhou, Z. X. Wu, *ACS Appl. Mater. Interfaces* **2019**, *11*, 16152-16164; (d) Z. Feng, D. Z. Wang, X. L. Yang, D. Y. Jin, Z. K. Zhong, B. O. Liu, G. J. Zhou, M. F. Ma, Z. X. Wu, *Inorg. Chem.* **2018**, *57*, 11027-11043; (e) X. L. Yang, H. R. Guo, B. O. Liu, J. Zhao, G. J. Zhou, Z. X. Wu, W.-Y. Wong, *Adv. Sci.* **2018**, *5*, 1701067; (f) W. P. Dang, X. L. Yang, Z. Feng, Y. H. Sun, D. K. Zhong, G. J. Zhou, Z. X. Wu, W.-Y. Wong, *J. Mater. Chem. C* **2018**, *6*, 9453-9464; (g) X. B. Xu, H. R. Guo, J. Zhao, B. O. Liu, X. L. Yang, G. J. Zhou, Z. X. Wu, *Chem. Mater.* **2016**, *28*, 8556-8569.

[16] (a) P.-L. T. Boudreault, M. A. Esteruelas, E. Mora, E. E. Oñate, J.-Y. Tsai, *Organometallics* **2019**, *38*, 2883-2887; (b) Y. Hisamatsu, S. Kumar, S. Aoki, *Inorg. Chem.* **2017**, *56*, 886-899; (c) Y. Tamura, Y. Hisamatsu, S. Kumar, T. Itoh, K. Sato, R. Kuroda, S. Aoki, *Inorg. Chem.* **2017**, *56*, 812-833.

[17] Y. Tamura, Y. Hisamatsu, A. Kazama, K. Yoza, K. Sato, R. Kuroda, S. Aoki, *Inorg. Chem.*, 2018, **57**, 4571-4589.

[18] V. Adamovich, S. Bajo, P.-L. T. Boudreault, M. A. Esteruelas, A. M. López, J. Martín, M. Oliván, E. Oñate, A. U. Palacios, A. San-Torcuato, J.-Y. Tsai, C. J. Xia, *Inorg. Chem.* **2018**, *57*, 10744-10760.

[19] J.-L. Liao, Y. Chi, Z.-T. Sie, C.-H. Ku, C.-H. Chang, M. A. Fox, P. J. Low, M.-R. Tseng, G.-H. Lee, *Inorg. Chem.* **2015**, *54*, 10811-10821.

[20] K.-H. Kim, J.-J. Kim, *Adv. Mater*. **2018**, *30*, 1705600.

[21] (a) J. S. Kim, D. Leong, H. J. Bae, Y. Jung, S. Nam, J. W. Kim, S.-G. Ihn, J. Kim, W.-J. Son, H. Choi, S. Kim, *Adv. Opt. Mater.* **2020**, *8*, 2001103; (b) A. K. Pal, S. Krotkus, M. Fontani, C. F. R. Mackenzie, D. B. Cordes, A. M. Z. Slawin, I. D. W. Samuel, E. Zysman-Colman, *Adv. Mater.* **2018**, *20*, 1804231.

[22] (a) C.-K. Moon, K.-H. Kim, J.-J. Kim, *Nat. Commun.* **2017**, *8*, 791; (b) M. J. Jurow, C. Mayr, T. D. Schmidt, T. Lampa, P. I. Djurovich, W. Brütting, M. E. Thompson, *Nat. Mater*. **2016**, *15*, 85-91.

[23] (a) C.-Y. Chen, W.-K. Lee, Y.-J. Chen, C.-Y. Lu, H. Y. Lin, C.-C. Wu, *Adv. Mater*. **2015**, *27*, 4883-4888; (b) L. H. Smith, J. A. E. Wasey, I. D. W. Samuel, W. L. Barnes, *Adv. Funct. Mater.* **2005**, *15*, 1839-1844.

[24] D. Wasserberg, S. C. J. Meskers, R. A, J. Janssen, *J. Phys. Chem. A* **2007**, *111*, 1381-1388.

[25] P.-N. Lai, C. H. Brysacz, M. K. Alam, N. A. Ayoub, T. G. Gray, J. Bai and T. S. Teets, *J. Am. Chem. Soc.* **2018**, *140*, 10198-10207.

[26] I. Shigeru, Y. Shigeyuki, M. Takeshi, N. Hiroyuki, F. Hideki, K. Shiro, S. Yoshiaki, *Inorg. Chem. Commun.* **2013**, *38*, 14-19.

[27] (a) D. R. Martir, E. Zysman-Colman, *Coord. Chem. Rev.* **2018**, *364*, 86-117; (b) L. Yin, C.-L. Ho, H. B. Wu, Y. Cao, W.-Y. Wong, *Adv. Mater.* **2014**, *26*, 2459-2473.

[28] X. L. Yang, G. J. Zhou, W.-Y. Wong, *Chem. Soc. Rev.* **2015**, *44*, 8484-8575.

[29] J. Song, H. Lee, E. G. Jeong, K. C. Choi, S. Yoo, *Adv. Mater.* **2020**, *32*, 1907539.

[30] X. Li, J. Zhang, Z. Zhao, L. Wang, H. Yang, Q. Chang, N. Jiang, Z. Liu, Z. Bian, W. Liu, Lu, C. Huang, *Adv. Mater.* **2018**, *30*, 1705005.

[31] S.-Y. Kim, W.-I. Jeong, C. Mayr, Y.-S. Park, K.-H. Kim, J.-H. Lee, C.-K. Moon, W. Brütting, J.-J. Kim, *Adv. Funct. Mater.* **2013**, *23*, 3896-3900.